APPLIED PHYSICS LETTERS **94**, 103106 (2009)

Optically pumped nanolaser based on two magnetic plasmon resonance modes

Z. H. Zhu,[1,2] H. Liu,[1,a)] S. M. Wang,[1] T. Li,[1] J. X. Cao,[1] W. M. Ye,[2] X. D. Yuan,[2] and S. N. Zhu[1,a)]

[1]*Department of Physics, National Laboratory of Solid State Microstructures, Nanjing University, Nanjing 210093, People's Republic of China*

[2]*College of Opto-Electronic Engineering, National University of Defense Technology, Changsha 410073, People's Republic of China*

(Received 15 November 2008; accepted 12 February 2009; published online 11 March 2009)

We propose and analyze theoretically a double magnetic plasmon resonance nanolaser, in which ytterbium-erbium codoped material is used as the gain medium. Through design of the double magnetic resonance modes, pumping light (980 nm) can be resonantly absorbed and laser light (1550 nm) can be resonantly generated simultaneously. We introduce a set of rate equations combined to describe the operation of the laser and predict the lasing condition. According to our calculations, the disadvantage that pumping light is difficult to be absorbed by a thin slab of gain materials can be overcome. © *2009 American Institute of Physics*. [DOI: 10.1063/1.3095437]

Reducing mode volume in cavities is very favorable for achieving strong light-matter interaction processes.[1] These strong interactions are of great benefit to applications in light emitting devices. Recently, in order to further miniaturize mode volume and physical size of the structure, researchers turn to use metal instead of dielectric to bound the mode field.[2–6] For example, a metallic-coated cavity formed by encapsulating a semiconductor heterostructure in a thin gold film is used to obtain mode volume far smaller than conventional dielectric cavities.[2] In addition, due to the strong localized surface plasmon effect, electromagnetic energy is also able to be highly confined in nanoscale.[3–6]

In 1999, Yen *et al.*[7] proposed the split-ring resonator to realize magnetic plasmon resonance in microwaves. Since then, scientists introduce many new structures to achieve magnetic resonance in high frequency region, such as fish net[8] and nanosandwich.[9] It is shown that such magnetic response structures offer a great promise for applications in negative refractions,[10–12] perfect lens,[13] subwavelength waveguides,[14] etc. Very recently, magnetic plasmon resonance is proposed as an efficient way to produce nanolasers.[15,16] However, to the best of our knowledge, all the structures up to now only resonate with the lasing light. In these structures, most of external energy is difficult to be absorbed by these nanocavities.

In this work, we design a metallic nanosandwich cavity, which can possess two magnetic plasmon resonance modes at two prescribed resonance wavelengths. Combined with the ytterbium-erbium codoped gain material Er:Yb:YCOB, this cavity can have resonance not only at lasing wavelength but also at pumping wavelength, which lead to efficient pump-laser conversion.

Figure 1(a) presents the proposed laser arrays constructed by immersing a regular array of rectangular silver slab in gain medium Er:Yb:YCOB, which is supported by a silver film and SiO_2 glass substrate. The geometry parameters of the structure shown in Figs. 1(b) and 1(c) are defined as follows: the immersed upper silver slab is a rectangular slab with a size of $310\times 245\times 50$ nm^3. The gap size between the immersed silver slab and bottom silver film is 50 nm. The thicknesses of the silver film, gain medium layer above the silver film, and SiO_2 glass substrate are 50, 250, and 250 nm, respectively. The permittivity of the silver is given by $\varepsilon(\omega)=\varepsilon_\infty-\omega_p^2/(\omega^2+i\omega/\tau)$. The values of ε_∞, ω_p, and τ fitted to experimental data in the 950–1800 nm wavelength range are 1.0, 1.38×10^{16} rad/s, and 33 fs, respectively. The refractive indices of Er:Yb:YCOB and SiO_2 substrates are measured to be 1.3 and 1.5, respectively.

In this paper, we focus on the lasing condition of a single magnetic resonator. The distance between the nearest-neighbor resonators is large enough (~1000 nm) and the coupling interaction among these resonators can be neglected. From Pendry's theory, the structure shown in Fig. 1(b) can be seen as an equivalent inductance-capacitance circuit. When magnetic resonance occurs, the electromagnetic energy is mainly stored in the space between the silver slab and film, so the structure can be considered as a cavity of confining light. One main character of magnetic resonance

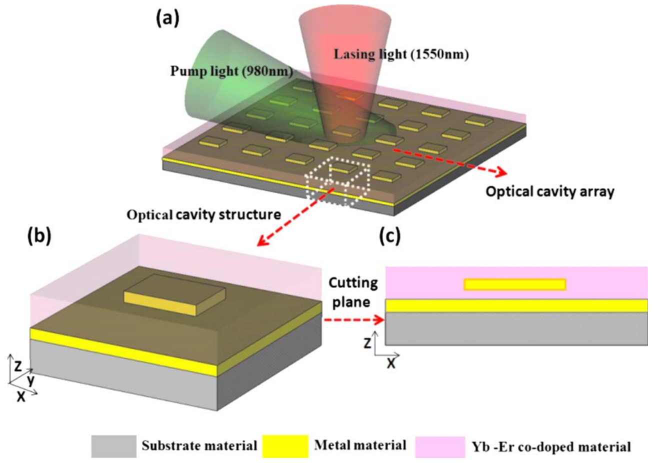

FIG. 1. (Color online) Metallic magnetic resonance nanolaser structures. (a) Laser arrays. (b) Single laser cell structure. (c) Cutting plane (*z*-*x* plane) of single laser cell structure.

---

[a] Authors to whom correspondence should be addressed. Electronic addresses: liuhui@nju.edu.cn and zhusn@nju.edu.cn.

0003-6951/2009/94(10)/103106/3/$25.00

© 2009 American Institute of Physics

Downloaded 12 Mar 2009 to 202.119.32.141. Redistribution subject to AIP license or copyright; see http://apl.aip.org/apl/copyright.jsp

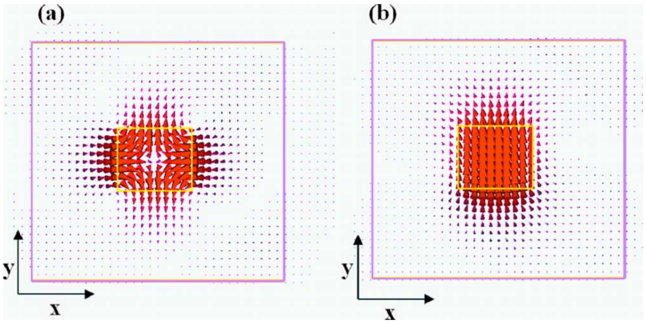

FIG. 2. (Color online) Magnetic field vectors of two magnetic resonance modes. (a) Corresponding to mode MP_{22}. (b) Corresponding to mode MP_{10}.

mode is that the induced current forms loops and strong magnetic fields inside them. For different magnetic resonance modes, a different number of loops is formed in the cavity. So, we can label one mode as MP_{ij}, where i and j denote the formed loop numbers along the x and y directions, respectively. It is found that the electric fields of mode MP_{10} and MP_{22} have quite a large spatial overlap, so these two modes are selected as the operation modes in our calculations. For the carefully designed geometry size in Fig. 1(b), the resonance wavelengths of the two modes are 980 and 1550 nm, respectively. Figure 2 shows the magnetic field vector distributions of the two modes in the middle dielectric layer. Figures 3(b) and 3(d) show respectively the electric field component Ey distributions for the two modes. As the 980 and 1550 nm are respectively close to the absorption peak and emission peak of Er:Yb:YCOB, we can select the higher order MP_{22} mode as the pumping mode (980 nm), and the lower MP_{10} mode as the lasing mode (1550 nm).

TABLE I. Parameters used in the calculations.

Parameters	Values	Notes
Q_l	50	Calculated by FDTD
Q_p	60	Calculated by FDTD
V_l	1.6×10^{-3}	Calculated by FDTD
V_p	4.0×10^{-2}	Calculated by FDTD
υ_l	2.3×10^{8} m/s	Calculated by FDTD
υ_p	2.1×10^{8} m/s	Calculated by FDTD
σ_E	5.0×10^{-25} m^2	See Ref. 18
σ_Y	8.0×10^{-25} m^2	See Ref. 18
τ_{2E}	5.0×10^{-3} s	See Ref. 18
τ_{2Y}	2.6×10^{-3} s	See Ref. 17
C	1.3×10^{-23} m^3/s	See Ref. 17
k_1,k_2	5.0×10^{-21} m^3/s	See Refs. 19 and 20

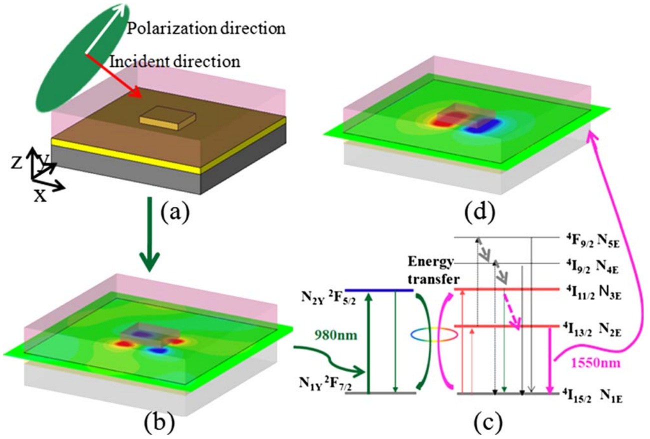

FIG. 3. (Color online) Schematic illustration of the operation principle of the laser. (a) Pumping light incident. (b) Resonantly pumping cavity mode (980 nm). (c) Energy level diagram for the Er–Yb codoped system. (d) Lasing cavity mode (1550 nm).

Figure 3 illustrates schematically the operation principle of the double magnetic resonance laser. To predict the lasing condition, we introduce a set of rate equations to model the operation of the laser. As we have known, if the radiative transition frequency of the atom or ion matches that of the resonance mode of a cavity, the rate of spontaneous or stimulated emission can be enhanced. The measure of the enhancement is the Purcell factor defined by $F=3Q\lambda^3/(4\pi^2Vn^3)$,[21,22] where n, λ, Q, and V are the refractive index of gain material, the wavelength, the quality factor, and the effective mode volume of laser mode, respectively. Here, the rate equations take into account enhanced spontaneous and stimulated emission. Namely, the absorption cross section of Yb^{3+} and emission cross section of Er^{3+} in the rate equations are $F_l\sigma_E$ and $F_p\sigma_Y$, respectively, where σ_Y and σ_E are the absorption cross section of Yb^{3+} and emission cross section of Er^{3+} in free space (here, "free space" as the meaning of "without cavity"). In addition, considering the localized property of the pumping and lasing modes, we also take into account the spatial distributions of two modes. The energy level diagram for the Er:Yb:YCOB is shown in Fig. 3(c). In steady-state conditions, neglecting both the populations in the levels $^4I_{11/2}$, $^4I_{9/2}$, and $^4F_{9/2}$ and corresponding back-transfer processes due to the fast nonradiative decay in these levels, the simplified rate equations and condition for threshold are expressed as[17,19]

$$\frac{\partial N_{2Y}}{\partial t}=0=\sigma_Y\upsilon_pF_pN_pf_p(N_{1Y}-N_{2Y})-k_1N_{2Y}N_{1E}-k_2N_{2Y}N_{2E}-\frac{N_{2Y}}{\tau_{2Y}}, \quad (1)$$

$$\frac{\partial N_{2E}}{\partial t}=0=k_1N_{2Y}N_{1E}-(N_{2E}-N_{1E})\upsilon_lF_l\sigma_EN_lf_l-\frac{N_{2E}}{\tau_{2E}}-2CN_{2E}^2, \quad (2)$$

$$\frac{\partial N_l}{\partial t}=0=\upsilon_lF_l\sigma_E\int\int\int(N_{2E}-N_{1E})N_lf_ldV-\frac{\omega_lN_l}{Q_l}, \quad (3)$$

where N_{ix} and τ_{ix} represent, respectively, the population density and lifetime of the corresponding levels shown in Fig. 2(c). k_1 and k_2 are the coefficients of the two energy transfer processes. C is the upconversion rate. ω_l is the angle frequency of lasing mode. υ_p, N_p, and f_p are the group velocity, total photon number, and normalized spatial intensity distributions of the higher order magnetic resonant mode (980 nm), respectively. υ_l, N_l, and f_l represent respectively the corresponding parameters of the lasing mode. f_p and f_l are normalized such that

$$\int\int\int f_pdV=1 \quad \text{and} \quad \int\int\int f_ldV=1, \quad (4)$$

where V is the volume. In addition, in steady-state conditions, it is reasonable to give these approximate expressions

$$N_{1E}+N_{2E}\approx N_E, \quad N_{1Y}\approx N_Y. \quad (5)$$

The properties of the two magnetic plasmon resonance modes, such as the quality factor (obtained by measuring the

Downloaded 12 Mar 2009 to 202.119.32.141. Redistribution subject to AIP license or copyright; see http://apl.aip.org/apl/copyright.jsp

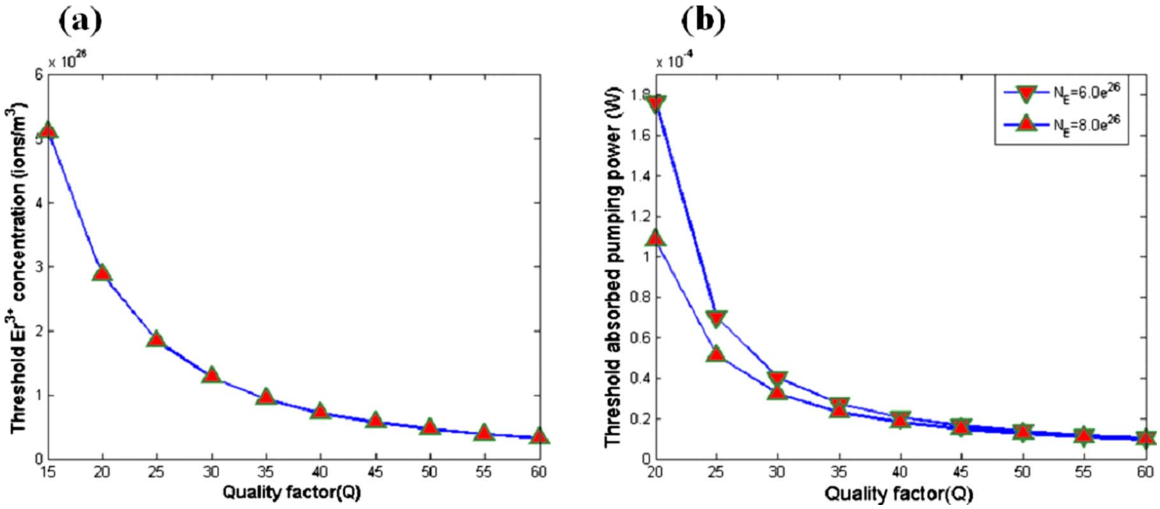

FIG. 4. (Color online) Threshold lasing condition. (a) Threshold Er^{3+} concentration plotted as a function of modified quality factor Q. (b) Absorbed threshold pumping power plotted as a function of modified quality factor Q at two different erbium concentrations.

rate of exponential decay of the electromagnetic energy for the given resonance mode), group velocity, effective mode volume, and normalized spatial intensity distributions, are calculated in our simulations and listed in Table I. The other material parameters used in the calculation are also included in Table I. In general, the Yb^{3+} concentration is an order of magnitude higher than Er^{3+} concentration. In our calculations, we fix the Yb^{3+} concentration at 5.0×10^{27} ions/m^3 and predict the threshold Er^{3+} concentrations. Substituting the pumping mode and lasing mode parameters into Eqs. (1)–(5), and assuming the total photon number of lasing mode in the cavity to be 1 and the pumping rate to be high enough, we can predict the Er^{3+} threshold doping concentrations to be 4.6×10^{25} ions/m^3. In our theoretical work, we consider the film influence on the property of metal material by reducing the quality factor of lasing mode, which corresponds to larger metallic losses in metallic film. Figure 4(a) shows the threshold doping concentration plotted as a function of modified quality factor Q of lasing mode. It can be seen from the figure, as the quality factor decreases, the threshold doping concentration increases. When Q is decreased from 50 to 15, the corresponding threshold Er^{3+} concentration is increased from 4.6×10^{25} to 5.1×10^{26} ions/m^3. Typical Er^{3+} concentration in Er:Yb:YCOB is in the range of $10^{25}-10^{27}$ ion/m^3. So, Er:Yb:YCOB can theoretically satisfy the operating condition of the metallic magnetic resonance nanolaser. Choosing Er^{3+} concentration at 6.0×10^{26} and 8.0×10^{26} ions/m^3, we calculate the corresponding absorbed threshold pumping power ($\hbar\omega_p\sigma_Y v_p F_p N_p N_Y/\eta_p$, η_p is the quantum efficiency and approximately equal to 1), respectively, as shown in Fig. 4(b). From Fig. 4(b), at a fixed Er^{3+} concentration, the absorbed threshold pumping power increases with the decrease in Q factor. This means that more metallic losses must be compensated by higher pumping power.

In summary, a metallic double magnetic plasmon resonance nanolaser has been proposed. Due to that both the pumping mode and the lasing mode are resonant in the cavity, the pumping efficiency can be enhanced greatly. The finite-difference time-domain (FDTD) method and a set of rate equations are introduced to model the operation of the laser and predict the lasing condition. Results prove that the proposed double resonance laser can work as a compact nanolaser with quite low threshold value.

This work is supported by these National Programs of China (Grant Nos. 10704036, 10604029, 10534020, and Grant No. 2006CB921804).

[1] J. M. Gérard, B. Sermage, B. Gayral, B. Legrand, E. Costard, and V. Thierry-Mieg, Phys. Rev. Lett. **81**, 1110 (1998).
[2] M. T. Hill, Y. S. Oei, B. Smalbrugge, Y. Zhu, T. de Vries, P. J. van Veldhoven, F. W. M. van Otten, T. J. Eijkemans, J. P. Turkiewicz, H. de Waardt, E. J. Geluk, S. H. Kwon, Y. H. Lee, R. Notzel, and M. K. Smit, Nat. Photonics **1**, 589 (2007).
[3] H. T. Miyazaki and Y. Kurokawa, Phys. Rev. Lett. **96**, 097401 (2006).
[4] E. Feigenbaum and M. Orenstein, Opt. Express **15**, 2607 (2007).
[5] C. Manolatou and F. Rana, IEEE J. Quantum Electron. **44**, 435 (2008).
[6] D. J. Bergman and M. I. Stockman, Phys. Rev. Lett. **90**, 027402 (2003).
[7] T. Y. Yen, W. J. Padilla, N. Fang, D. C. Vier, D. R. Smith, J. B. Pendry, D. N. Basov, and X. Zhang, Science **303**, 1494 (2004).
[8] S. Zhang, W. Fan, N. C. Panoiu, K. J. Malloy, R. M. Osgood, and S. R. J. Brueck, Phys. Rev. Lett. **95**, 137404 (2005).
[9] V. M. Shalaev, W. Cai, U. K. Chettiar, H.-K. Yuan, A. K. Sarychev, V. P. Drachev, and A. V. Kildishev, Opt. Lett. **30**, 3356 (2005).
[10] G. Dolling, C. Enkrich, M. Wegener, C. M. Soukoulis, and S. Linden, Science **312**, 892 (2006).
[11] D. R. Smith, J. B. Pendry, and M. C. K. Wiltshire, Science **305**, 788 (2004).
[12] A. N. Grigorenko, A. K. Geim, H. F. Gleeson, Y. Zhang, A. A. Firsov, I. Y. Khrushchev, and J. Petrovic, Nature (London) **438**, 335 (2005).
[13] N. Fang, H. Lee, C. Sun, and X. Zhang, Science **308**, 534 (2005).
[14] H. Liu, D. A. Genov, D. M. Wu, Y. M. Liu, J. M. Steele, C. Sun, S. N. Zhu, and X. Zhang, Phys. Rev. Lett. **97**, 243902 (2006).
[15] N. I. Zheludev, S. L. Prosvirnin, N. Papasimakis, and V. A. Fedotov, Nat. Photonics **2**, 351 (2008).
[16] A. K. Sarychev and G. Tartakovsky, Phys. Rev. B **75**, 085436 (2007).
[17] P. A. Burns, J. M. Dawes, P. Dekker, J. A. Piper, H. Jiang, and J. Wang, IEEE J. Quantum Electron. **40**, 1575 (2004).
[18] P. Wang, J. M. Dawes, P. Burns, J. A. Piper, H. Zhang, L. Zhu, and X. Meng, Opt. Mater. (Amsterdam, Neth.) **19**, 383 (2002).
[19] E. Yahel and A. Hardy, J. Lightwave Technol. **21**, 2044 (2003).
[20] S. Bjurshagen, J. E. Hellström, V. Pasiskevicius, M. C. Pujol, M. Aguiló, and F. Díaz, Appl. Opt. **45**, 4715 (2006).
[21] S. A. Maier, Opt. Quantum Electron. **38**, 257 (2006).
[22] H. Y. Ryu and M. Notomi, Opt. Lett. **28**, 2390 (2003).

Downloaded 12 Mar 2009 to 202.119.32.141. Redistribution subject to AIP license or copyright; see http://apl.aip.org/apl/copyright.jsp